This article has been accepted for publication in IEEE Transactions on Consumer Electronics. This is the author's version which has not been fully edited and content may change prior to final publication. Citation information: DOI 10.1109/TCE.2026.3675966

Consumer-Electronics-Oriented Safe Interaction-Aware Motion Planning for Ramp Driving with Perception Uncertainty Quantification

Zhen Tian[1,†], Zhihao Lin[1,†], Chunhong Yuan[2], Sunil Prajapat[3], *Member, IEEE*, Jing Yang[4,§], and Por Lip Yee[4], *Senior Member, IEEE*

***Abstract*—Autonomous ramp driving is challenging due to complex interactions between autonomous vehicles (AVs) and human-driven vehicles (HDVs) with diverse driving styles, as well as strict geometric constraints imposed by ramp terminations. For consumer electronic vehicles (CEVs), these challenges are further amplified by limited computational resources and real-time decision requirements. This paper proposes a consumer-electronics-oriented cooperative motion planning framework for autonomous ramp driving that integrates driving style awareness, perception uncertainty quantification, and interaction-aware decision-making. Heterogeneous HDV behaviors are modeled using data-driven driving style classification, while prediction uncertainty is captured via error ellipses. A game-theoretic formulation is employed to select lane-changing time points, which are then translated into executable trajectories through lightweight planning and control modules. Simulation results based on the NGSIM dataset and diverse ramp traffic scenarios demonstrate collision-free operation with improved merge efficiency and velocity smoothness under varying traffic densities. Furthermore, a dedicated consumer electronics platform evaluation shows that the proposed method achieves sub-millisecond runtime, minimal memory usage, and low energy consumption, outperforming several recent 2025 state-of-the-art planners, including mean-field-game-based MPC, Monte Carlo decision processes, and risk-field-based game-theoretic approaches. These results indicate that the proposed framework is well suited for safe and efficient ramp driving on consumer-grade autonomous vehicle platforms.**

***Index Terms*—Autonomous driving, consumer electric vehicles, driving styles, interactive driving, lane changing, uncertainty quantification.**

I. INTRODUCTION

AUTONOMOUS ramp driving is among the most challenging scenarios for electric and intelligent vehicles (EIVs), due to dense traffic, limited merging space, and strong interactions with human-driven vehicles (HDVs). Safe ramp merging requires precise timing and robust decision-making under dynamic traffic conditions. Meanwhile, autonomous vehicles are increasingly deployed on consumer-grade platforms with compact ECUs, efficient processors, and sensor-rich perception, imposing strict constraints on real-time computation, memory, and energy. Here, *consumer-grade platforms* refer to embedded automotive systems with limited onboard resources.

Key challenges further arise from diverse human driving styles and ramp-end geometric constraints requiring timely lane changes. To navigate effectively, AVs must recognize and predict surrounding behaviors and adapt to lane configurations and intentions [1]. This paper investigates interaction-aware ramp driving for EIVs, enabling AVs to cooperate with HDVs under embedded consumer systems integrating perception, decision, and control. The proposed framework ensures smooth and safe ramp merging under complex traffic conditions [2].

Human drivers may focus on safety, efficiency, or comfort [3], making strategy-modeling essential for effective interaction with HDVs. Existing methods for interaction with HDVs are reviewed in [4], covering scenarios such as car following and lane changing. The Intelligent Driving Model (IDM) [5] is commonly used for car-following phase, as it replicates realistic driving behaviors like smooth acceleration and collision avoidance. IDM also improves safety and efficiency compared to human driving [6]. During lane changing, predictions of surrounding vehicles' motions and intentions are required. Game-theoretic approaches [7] address this but often assume full knowledge of others' strategies, which is unrealistic without driving style classification [8]. Additionally, most studies overlook perception and prediction uncertainties, which can undermine decision reliability. During ramp merging, the AV must decide when to merge based on predictions of surrounding HDVs' motions and intentions. Game-theoretic approaches offer a principled interaction model; however, without explicit driving style and uncertainty modeling, they may yield unrealistic or unsafe decisions.

Uncertainty-aware motion models [9], [10], [11] and error ellipse methods [12], [13] help improve trajectory prediction by capturing motion uncertainties. Once predictions are obtained, the AV selects an optimal lane-changing time using equilibrium theory [14]. This enables interaction-aware decision-making under uncertainty. Utility-based approaches [15] further enhance decision-making by incorporating predicted trajectories and their uncertainties. The selected time point of lane-changing can then be used for vehicle path

*This work was supported by the Bantuan Khas Penyelidikan (BKP Special) (BKP051-2024-ECRG), the University Grant (UMG009D-2025) at Universiti Malaya, Malaysia, and the National Science and Technology Council in Taiwan under Grant No. NSTC-114-2224-E-027-001.

Zhen Tian, and Zhihao Lin are with James Watt School of Engineering, University of Glasgow, Glasgow G12 8QQ, United Kingdom

[2]Faculty of Control Systems and Robotics, ITMO University , St. Petersburg, 197101, Russia

Sunil Prajapat is with the Deptartment of Computer Engineering-AI Big Data, Marwadi University, 360006 India.

[4] Jing Yang, and Por Lip Yee are with Center of Research for Cyber Security and Network (CSNET), Faculty of Computer Science and Information Technology, Universiti Malaya, 50603 Kuala Lumpur, Malaysia

[§]Corresponding author. Jing Yang(e-mail: s2147529@siswa.um.edu.my)

† Equal contribution

planning by using the interpolation method [16].

Driving style diversity plays a critical role in ramp driving, as human drivers may prioritize safety, efficiency, or comfort differently. Existing studies on driving style recognition mainly focus on car-following or isolated lane-changing behaviors, while interactive dynamics with surrounding vehicles are often overlooked. Fixed or static grading schemes further limit adaptability in highly dynamic merging scenarios. Recent studies have explored interactive ramp driving. [17] formulates ramp merging as a Stackelberg game for connected automated vehicles in mixed traffic, but does not account for perception uncertainty or heterogeneous driving style classification. [18] and [19] investigate cooperative lane-changing strategies for connected autonomous vehicles merging into dedicated lanes under mixed traffic conditions; however, they focus on platoon-level coordination rather than individual-level interaction-aware decision-making with driving style diversity. [20] uses a game-based approach but overlooks prediction uncertainty and lacks real-world driving style data. [21] proposes a cooperative merging strategy for a basic two-lane ramp, ignoring the impact of other lanes and assuming fixed vehicle lengths. [22] simulates CAV-HDV interactions under varying traffic densities, but its simplified setup omits realistic driving styles and behaviors. In contrast, our method considers these factors, such as AV lane changes in response to unsatisfied HDVs. [23] proposes a sampling-based solver for generalized Nash equilibrium with interacting vehicle isolation. However, the evaluation is limited to a single road and ramp scenario and does not consider prediction errors [24].

To tackle these challenges, we propose a **consumer-electronics-oriented top-down planner** for ramp driving, enabling AVs to interact intelligently with surrounding vehicles exhibiting diverse driving styles. The proposed framework integrates three components: a scoring-based driving style grader, a game-theoretic time point selector based on error ellipses, and a high-resolution path planner optimized for embedded electronic platforms. The main contributions are:

- **Robust top-to-down on-ramping framework:** The proposed framework integrates interaction-aware decision-making, uncertainty quantification, and consumer-grade computational constraints into a unified ramp-driving planner, enabling safe and efficient operation under dense mixed-traffic conditions.
- **Consumer-level driving style recognition:** A real-world data–driven style classifier is designed using ITTC and THW metrics [25], enabling the system to identify human driving styles and select ramp entry points that balance intentions while minimizing prediction errors.
- **Integrated dissatisfaction-aware coordination:** The planner jointly evaluates heterogeneous HDV types and lane-changing intentions through a dissatisfaction measure, reflecting human-like comfort perception and cooperation, an aspect that has been largely overlooked in previous consumer-oriented driving frameworks.
- **Validated consumer-intelligent performance:** Simulations with diverse HDVs and ramp traffic conditions show that the proposed system achieves zero collisions, shorter merge-to-exit times, higher velocity profiles, and improved throughput, confirming suitability for embedded consumer vehicle platforms.

II. Problem Statement and System Overview

Autonomous ramp driving requires AVs to interact and coordinate with surrounding HDVs exhibiting diverse driving styles, while satisfying strict spatial and temporal constraints imposed by the ramp geometry.

1) Interactive traffic environment: In the ramp scenario, the AV must complete its lane change before the ramp ends, after which merging is no longer possible. Therefore, it must make timely, interaction-aware decisions based on surrounding traffic and inferred driving styles of neighboring vehicles.

To reflect realistic traffic behavior, multiple vehicle intentions are modeled. Specifically, surrounding vehicles may exhibit different interaction patterns depending on available space ahead. When sufficient longitudinal gap exists, vehicles tend to interact cooperatively with the AV. In contrast, when space is limited, vehicles are more likely to adopt defensive or aggressive behaviors, prioritizing safety and gap preservation.

To capture this effect, we introduce an unsatisfactory level that quantifies a vehicle's incentive to change lanes:

$$L_{\text{unsat}} = w_{\text{gap}} \cdot s_{\text{adj}}/s_{\text{front}} + w_{\text{vel}} \cdot v_{\text{self}}/v_{\text{front}}, \tag{1}$$

where w_{gap} and w_{vel} are weighting factors. Here, s_{adj} and s_{front} denote the available front gaps in the adjacent and current lanes, respectively, while v_{self} and v_{front} represent the velocities of the subject vehicle and its preceding vehicle in the same lane. When L_{unsat} exceeds a predefined threshold, the vehicle initiates a lane change, with left-lane changes preferred under typical driving behavior. In this work, we set $w_{\text{gap}} = 0.8$ and $w_{\text{vel}} = 0.2$, placing greater emphasis on gap adequacy due to its direct safety impact during lane changes. These values were empirically validated across different traffic densities, yielding consistent triggering behavior.

2) Vehicle model: For efficient multi-agent decision-making, we adopt the kinematic bicycle model for AV control:

$$\dot{x} = v\cos(\varphi), \quad \dot{y} = v\sin(\varphi), \quad \dot{\varphi} = v\tan(\delta)/L, \tag{2}$$

where x and y denote the longitudinal and lateral positions of the vehicle, φ is the heading angle, L is the wheelbase, and v and δ are the control inputs representing velocity and steering angle, respectively. The model in (2) is well suited for low-speed ramp driving, where lateral dynamics and tire slip effects are limited. Although higher-fidelity dynamic models are required at high speeds, the adopted kinematic model offers an effective balance between modeling accuracy and computational efficiency for interaction-aware decision-making in dense ramp environments.

3) Proposed interactive ramp driving system: We propose an interactive ramp driving framework integrating driving style assessment, uncertainty quantification, and game-theoretic decision-making. As illustrated in Fig. 1, it consists of four layers: driving style classification, uncertainty quantification, decision-making, and motion planning/control.

The driving style layer infers behavioral tendencies of surrounding HDVs, the uncertainty quantification layer models

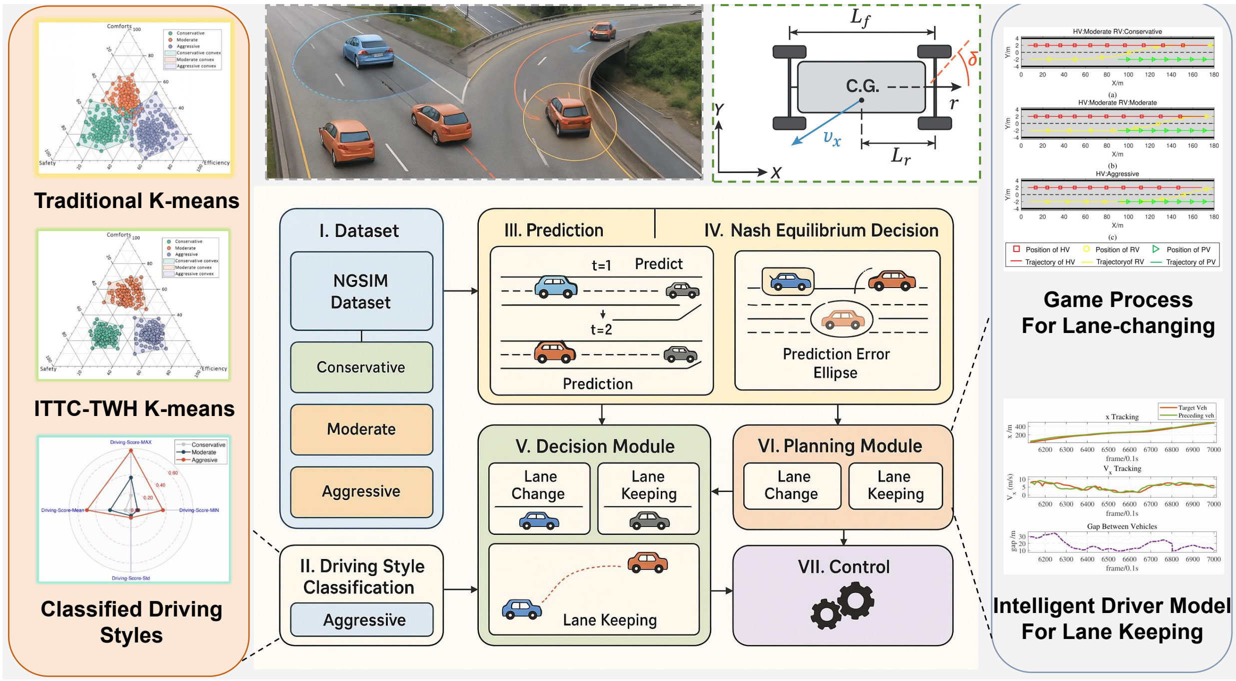

Fig. 1: The interactive ramp driving workflow, with stages III to VII detailed in their respective sections.

perception and prediction errors using error ellipses, and the decision layer selects an optimal lane-changing time point based on a game-theoretic formulation. Finally, the planning and control layer generates executable trajectories that satisfy vehicle dynamics and safety constraints. Detailed descriptions of each module are provided in Sections III–VII.

III. Classification of Driving Styles

Driving styles play a critical role in interactive decision-making, as human drivers exhibit different priorities with respect to safety, efficiency, and comfort [26], [27]. Conservative drivers tend to prioritize safety and maintain larger gaps, aggressive drivers emphasize efficiency and higher speeds, while moderate drivers balance these objectives. Accurately identifying such behavioral tendencies is therefore essential for interaction-aware ramp driving.

In this work, driving styles are inferred from real-world human driving data extracted from the NGSIM dataset. To ensure interpretability and robustness, we adopt two widely used traffic metrics: Inverse Time-To-Collision (ITTC) and Time Headway (THW), defined as

$$\mathrm{ITTC} = S/v_h, \qquad \mathrm{THW} = v_r/(S - L_p), \tag{3}$$

where S denotes the distance between the host and preceding vehicles, v_h is the host vehicle (HV) speed, v_r is the relative speed, and L_p is the length of the preceding vehicle. ITTC quantifies potential collision risk under constant-velocity assumptions, while THW reflects the temporal spacing between vehicles. Together, these metrics capture complementary aspects of driving aggressiveness and safety.

Based on established thresholds [25], ITTC values of 0.28 and 0.5 correspond to collision-free and high-risk conditions, respectively, while THW thresholds of 2 and 6 distinguish low-risk and comfortable following behaviors. Using these thresholds, driving behaviors are mapped into comfort, safety, and efficiency regions, as illustrated in Fig. 2.

To obtain a compact and quantitative representation, we define a driving score as

$$f_{\text{driving-score}} = w_1 P_{\text{comfort}} + w_2 P_{\text{safety}} + w_3 P_{\text{efficiency}}, \tag{4}$$

where P_{comfort}, P_{safety}, and $P_{\text{efficiency}}$ denote the proportions of time spent in each region, and w_1, w_2, and w_3 are user-defined weights. Higher scores indicate more aggressive driving styles, while lower scores correspond to conservative behaviors.

Using this representation, we extract 344 trajectories from the NGSIM dataset that satisfy minimum distance and duration requirements. Each trajectory is encoded as a three-dimensional feature vector and clustered using k-means to identify three distinct driving styles: conservative, moderate, and aggressive.

We adopt k-means since the driving score features are low-dimensional and the cluster number is known *a priori*. Moreover, k-means incurs minimal computational overhead, making it suitable for consumer-grade platforms; other methods such as Gaussian Mixture Models and Density-Based Spatial Clustering of Applications with Noise yielded comparable results at higher computational cost.

The resulting clusters exhibit clear separation and consistent statistical properties, as shown in Table I and Fig. 2, confirming the effectiveness of the proposed classification approach.

IV. Uncertainty Quantification

Quantifying uncertainty is vital for ramp driving to avoid potential risks. This paper uses an error ellipse based on an Axis-Aligned Gaussian model to represent prediction uncertainty. Given predicted positions $(x_p(t), y_p(t))$ and actual

This article has been accepted for publication in IEEE Transactions on Consumer Electronics. This is the author's version which has not been fully edited and content may change prior to final publication. Citation information: DOI 10.1109/TCE.2026.3675966

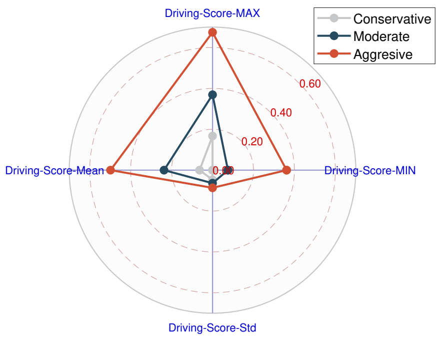

Fig. 2: Classification of driving styles based on driving scores.

TABLE I: DRIVING STYLES v.s. DRIVING SCORE

Driving Style	Driving Score			
	Max	Min	Mean	Standard Deviation
Aggressive	0.96	0.12	0.71	0.51
Moderate	0.53	0.09	0.34	0.11
Conservative	0.24	0.07	0.09	0.02

positions $(x(t), y(t))$, the associated covariance matrix defines the uncertainty area around each vehicle is

$$\Sigma = \mathrm{diag}(\delta_{\mathrm{xx}}^2, \delta_{\mathrm{yy}}^2), \tag{5}$$

with $\delta_{\mathrm{xx}}^2 = \frac{\sum_{t=1}^{T}(x_p(t)-\bar{x})^2}{T-1}$ and $\delta_{\mathrm{yy}}^2 = \frac{\sum_{t=1}^{T}(y_p(t)-\bar{y})^2}{T-1}$, where T is the time interval, $\bar{x}$ and $\bar{y}$ are the mean longitudinal and lateral positions over T.

Error variances are used to define the uncertainty area. A Chi-Square model, aligned with the Gaussian assumption, is applied to construct the error ellipse as follows:

$$(a_{\mathrm{ob}} - a_{\mathrm{eq}})^2/a_{\mathrm{eq}}^2 + (b_{\mathrm{ob}} - b_{\mathrm{eq}})^2/b_{\mathrm{eq}}^2 = s, \tag{6}$$

where a_{ob} and b_{ob} are observed sample counts, a_{eq} and b_{eq} are expected counts, and s is a constant value. Assuming $x \gg \delta_{xx}^2$, $(x - \delta_{xx})^2 \approx x^2$, similarly for y. This leads to the following error ellipse formulation: $x^2/\delta_{\mathrm{xx}}^2 + y^2/\delta_{\mathrm{yy}}^2 = s$. The 95% confidence factor is taken as a Chi-Square value to construct the error ellipse. In the simulation, the error ellipse lengths are set to 1.47,m and 0.18,m for the major and minor axes, respectively, following [12].

Remark on real-world deployment: We adopt an axis-aligned Gaussian model for efficiency on consumer platforms, but it cannot capture correlated or non-Gaussian perception uncertainties (e.g., occlusion or sensor noise). In practice, robustness improves by enlarging the safety buffer, e.g., augmenting d_{safe} with an additional margin scaling with prediction horizon and traffic density.

V. Decision-Making Process

A. Game Theory

We model the lane-changing interaction between the HV and the rear vehicle (RV) in the target lane as a two-player non-cooperative game. Each vehicle adopts a driving style (conservative, moderate, or aggressive), which determines the relative importance of safety, efficiency, and comfort in its decision-making. The game-theoretic formulation is used as a decision consistency mechanism rather than a centralized optimization tool, ensuring that a lane-changing decision is rational given the anticipated reactions of surrounding vehicles. In this game, the HV chooses between lane keeping (LK) and lane changing (LC), while the RV decides whether to cooperate (CO) or not cooperate (NC). Payoffs are defined for each action pair, and the equilibrium solution characterizes mutually consistent decisions under interaction and uncertainty.

1) Payoffs of HV: The HV's total payoff is defined as a weighted combination of safety, efficiency, and comfort:

$$P_{HV} = w_s^{\mathrm{HV}} P_s^{\mathrm{HV}} + w_e^{\mathrm{HV}} P_e^{\mathrm{HV}} + w_c^{\mathrm{HV}} P_c^{\mathrm{HV}}. \tag{7}$$

To unify lane-keeping and lane-changing cases, we introduce the binary vector $[\alpha, \beta]$, defined as

$$[\alpha, \beta] = \begin{cases} [1, 0], & \text{lane keeping}, \\ [0, 1], & \text{lane changing}. \end{cases} \tag{8}$$

The safety payoff of the HV is defined as

$$P_s^{\mathrm{HV}} = \alpha P_s^{\mathrm{HV,LK}} + \beta P_s^{\mathrm{HV,LC}}, \tag{9}$$

where

$$P_s^{\mathrm{HV,LK}} = 1, \quad P_s^{\mathrm{HV,LC}} = \frac{v_{\mathrm{HV}}\, s_{\mathrm{HV,RV}}}{(v_{\mathrm{HV}} + v_{\mathrm{RV}})(s_{\mathrm{HV,RV}} + d_{\mathrm{safe}} + \varepsilon_u r)}. \tag{10}$$

This formulation penalizes unsafe lane changes by jointly accounting for relative speed, inter-vehicle distance, and longitudinal prediction uncertainty modeled via the error ellipse radius r.

The efficiency payoff evaluates the ability of the HV to maintain its desired speed and is defined as

$$P_e^{\mathrm{HV}} = \alpha P_e^{\mathrm{HV,LK}} + \beta P_e^{\mathrm{HV,LC}}, \tag{11}$$

with

$$\begin{aligned} P_e^{\mathrm{HV,LK}} &= \frac{v_{\mathrm{HV}}}{v_{\mathrm{HV}} + \varepsilon_{\mathrm{FV}} v_{\mathrm{FV}}} \cdot \frac{1}{1 + \lambda_{\mathrm{CE}}\, C_{\mathrm{HV}}}, \\ P_e^{\mathrm{HV,LC}} &= \frac{v_{\mathrm{HV}}}{v_{\mathrm{HV}} + \varepsilon_{\mathrm{LV}} v_{\mathrm{LV}}} \cdot \frac{1}{1 + \lambda_{\mathrm{CE}}\, C_{\mathrm{HV}}}. \end{aligned} \tag{12}$$

where C_{HV} denotes a normalized consumer-electronics computational cost associated with the decision cycle, defined as a lightweight proxy proportional to runtime and energy consumption on embedded platforms, and λ_{CE} is a scaling factor balancing traffic efficiency and computational efficiency. The comfort payoffs of HV is formulated as

$$P_c^{\mathrm{HV}} = \alpha P_c^{\mathrm{HV,LK}} + \beta P_c^{\mathrm{HV,LC}}, \tag{13}$$

where $P_c^{\mathrm{HV,LK}}$ and $P_c^{\mathrm{HV,LC}}$ are HV's comfort payoffs during lane keeping and lane changing, formulated as

$$P_c^{\mathrm{HV,LK}} = P_c^{\mathrm{HV,LC}} = 1 - \triangle a_{\mathrm{HV}}/(a_{\max} - a_{\min}), \tag{14}$$

where $a_{\max}$ and $a_{\min}$ are maximum and minimum accelerations. Δa_{HV} is the acceleration difference between consecutive time steps. The comfort payoff function evaluates ride smoothness based on Δa_{HV}, normalized by $a_{\max} - a_{\min}$, with higher values indicating smoother driving.

This article has been accepted for publication in IEEE Transactions on Consumer Electronics. This is the author's version which has not been fully edited and content may change prior to final publication. Citation information: DOI 10.1109/TCE.2026.3675966

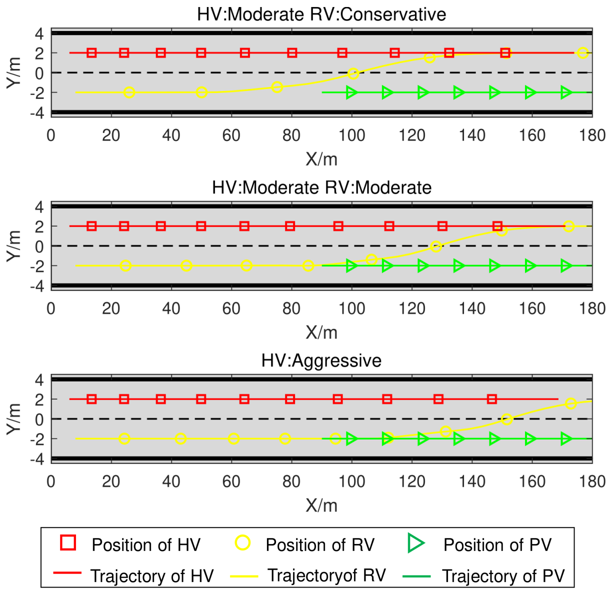

Fig. 3: Demo of interacting with three different driving styles.

2) Payoffs of RV: The RV adopts the same payoff structure as the HV, consisting of safety, efficiency, and comfort components:

$$P_{RV} = w_s^{\text{RV}} P_s^{\text{RV}} + w_e^{\text{RV}} P_e^{\text{RV}} + w_c^{\text{RV}} P_c^{\text{RV}}. \tag{15}$$

The RV's decision is represented by the binary vector $[\gamma, \zeta]$, corresponding to cooperation (CO) or non-cooperation (NC) with the HV.

The safety payoffs of RV is formulated as

$$P_s^{\text{RV}} = \gamma P_s^{\text{RV,CO}} + \zeta P_s^{\text{HV,NC}}, \tag{16}$$

where $P_s^{\text{RV,CO}}$ and $P_s^{\text{RV,NC}}$ denote RV's safety payoffs when cooperating or not cooperating with HV, defined as

$$P_s^{\text{RV,CO}} = P_s^{\text{RV,NC}} = \alpha P_s^{\text{HV,LK}} + \beta P_s^{\text{HV,LC}}, \tag{17}$$

where $P_s^{\text{RV,CO}}$ and $P_s^{\text{RV,NC}}$ are influenced by RV's decision. The RV's safety payoff mirrors HV's, with identical models for both cooperation and non-cooperation since avoiding collision with HV is the key concern in both cases.

The efficiency payoffs of RV is formulated as

$$P_e^{\text{RV}} = \gamma P_e^{\text{RV,CO}} + \zeta P_e^{\text{HV,NC}}, \tag{18}$$

where $P_s^{\text{RV,CO}}$ and $P_s^{\text{RV,NC}}$ represent RV's efficiency payoffs when cooperating or not with HV, defined as follows:

$$P_e^{\text{RV,CO}} = \frac{v_{\text{RV}}}{v_{\text{RV}} + \varepsilon_{\text{HV}} v_{\text{HV}}}, \quad P_e^{\text{RV,NC}} = \frac{v_{\text{RV}}}{v_{\text{RV}} + \varepsilon_{\text{LV}} v_{\text{LV}}} \tag{19}$$

where v_{RV} is the velocity of RV and ε_{HV} is the accommodation coefficient of HV. The efficiency payoff for RV reflects its ability to maintain desired speed. For $P_e^{\text{RV,CO}}$, it's based on HV due to potential speed adjustments, while for $P_e^{\text{RV,NC}}$, it depends on the LV ahead.

The payoffs of comfort is formulated as

$$P_c^{\text{RV}} = \gamma P_c^{\text{RV,CO}} + \zeta P_c^{\text{HV,NC}}, \tag{20}$$

where $P_c^{\text{RV,CO}}$ and $P_c^{\text{RV,NC}}$ are the comfort payoffs during cooperation and non-cooperation with HV, defined as

$$P_c^{\text{RV,CO}} = P_c^{\text{RV,NC}} = 1 - \frac{\triangle a_{\text{RV}}}{a_{\max} - a_{\min}}, \tag{21}$$

where Δa_{RV} is the acceleration difference. The comfort payoff, identical for both scenarios, rewards smoother acceleration with higher values.

3) Payoff weight configuration: The payoff weights w_s, w_e, and w_c balance safety, efficiency, and comfort. For the AV, three adaptive modes are defined by the available front gap: conservative $\{0.33, 0.33, 0.33\}$, balanced $\{0.5, 0.3, 0.2\}$, and aggressive $\{0.7, 0.2, 0.1\}$, with higher safety emphasis under smaller gaps. For HDVs, weights are randomly sampled between $\{0.33, 0.33, 0.33\}$ and $\{0.66, 0.66, 0.66\}$ to capture behavioral variability while avoiding extreme actions. These values were calibrated in simulation (Section VIII) and yield realistic interactions across traffic conditions.

4) Nash equilibrium: Nash equilibrium describes a state where each player selects their optimal strategy given the other's choice. Assuming RV's strategy is fixed (cooperate or not), HV selects the best response to maximize its payoff. The equilibrium is defined as

$$\Pi_{\text{HV}}^* := arg \max_{\pi \in \Pi} P_{\text{HV}}(\pi) = \{\pi^* \in \Pi : f(\pi^*) \geq f(\pi), \pi \in \Pi\},$$

where Π_{HV}^* is HV's optimal strategy (lane changing or keeping), π is a strategy and Π is the set of all strategies. At Nash equilibrium, both HV and RV adjust their decisions based on their combined driving styles. As shown in Fig. 3, HV has a moderate style, while RV's style ranges from conservative to aggressive, influencing HV's lane-changing behavior.

B. Feasibility Check of Lane Changing

Before the planning stage, the final step is to check the feasibility of the lane-changing maneuver. This ensures that the decision is safe despite uncertainties. Assuming the RV maintains a constant speed during lane changing, we generate a virtual smooth lane-change trajectory for short-horizon feasibility checking. This simplification is reasonable over the brief maneuver window (3–5 s) and is corrected by replanning at each cycle, while residual errors are accounted for by the uncertainty ellipse model (Section IV). A cubic polynomial, which offers simplicity, flexibility, and smoothness, is employed for this feasibility check, given by

$$y(x) = a_0 + a_1 x + a_3 x^2 + a_3 x^3, \tag{22}$$

where a_0, a_1, a_2 and a_3 are constant coefficients.

The lane-changing process is shown in Fig. 4, with a road width of 4 meters and three positions: $(0, -2)$, $(x_r, 0)$, and $(2x_r, 2)$. The risk point for the feasibility check is at (x_c, y_c). Substituting these positions into (22) gives: $a_0 = -2$, $a_0 + a_1 x_r + a_2 x_r^2 + a_3 x_r^3 = 0$, $a_0 + 2a_1 x_r + 4a_2 x_r^2 + 8a_3 x_r^3 = 2$. These are simplified as $a_1 = 2a_3 x_r^2$, $a_2 = -3a_3 x_r^2$ and $a_3 = 1/x_r^3$. Therefore, the cubic polynomials is obtained as

$$y(x) = -2 + 2x/x_r - 3x^2/x_r^2 + x^3/x_r^3.$$

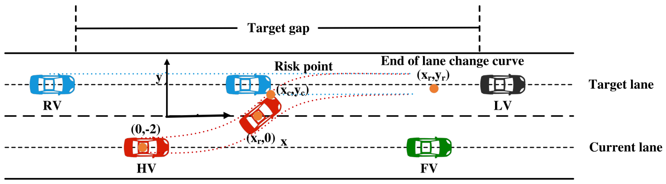

Fig. 4: Collision detection of lane changing.

The distance from the starting position to the risk position d_r is computed as

$$d_r = \int_0^{x_r} \sqrt{1+(y')^2}dx = \int_0^{x_r} \sqrt{1+(\frac{2}{x_r}+\frac{6x}{x_r^2}-\frac{6x^2}{x_r^3})^2}\,dx.$$

The time to risk (TTR) for RV and HV is computed as: $TTR_{\text{HV}} = d_r/v_{\text{HV}}$, $TTR_{\text{RV}} = x_r/v_{\text{RV}}$, where v_{HV} and v_{RV} are vehicle velocities at the starting position. The feasibility of lane changing is checked using

$$|TTR_{\text{HV}} - TTR_{\text{RV}}| > T_{\text{safe}}, \tag{23}$$

where T_{safe} is the safety time margin. The absolute value indicates that either HV or RV can reach the risk position first. As long as they have enough time difference, the lane change is considered safe.

VI. Planning

The planning module generates executable vehicle trajectories based on the decision outcome from the game-theoretic layer. Two planning modes are considered: lane keeping and lane changing.

If lane keeping is selected, longitudinal motion is planned using the Intelligent Driver Model (IDM), which regulates acceleration to maintain a safe and comfortable distance from the front vehicle (FV). If lane changing is selected and the feasibility check is satisfied, a smooth lateral maneuver is generated using an interpolation-based trajectory planner.

1) Longitudinal Planning via IDM: For lane keeping, the acceleration of the HV is computed using the IDM:

$$a_{\text{IDM}} = a_{\max}\Big[1-(v_{\text{HV}}/v_e)^4-(s^*/s)^2\Big]. \tag{24}$$

where $a_{\max}$ is the maximum acceleration, v_{HV} is the current velocity of the HV, v_e is the desired velocity, and s is the actual gap to the FV. The desired gap s^* is defined as

$$s^* = s_e + v_{\text{HV}}T_e - 0.5\cdot v_{\text{HV}}\Delta v/\sqrt{a_{\max}b}, \tag{25}$$

where s_e is the minimum desired spacing, T_e is the desired time headway, Δv is the relative velocity between the HV and FV, and b is the comfortable deceleration. This formulation ensures collision avoidance while maintaining smooth longitudinal behavior.

2) Lane-Change Trajectory Generation: When lane changing is selected, a geometric interpolation method is used to generate a smooth trajectory between the start point $(x_{\text{start}}, y_{\text{start}})$ and the target endpoint $(x_{\text{end}}, y_{\text{end}})$. The lateral displacement is determined by the lane geometry, while the longitudinal displacement is adjusted according to the vehicle speed to ensure ride comfort:

$$s_{\text{lon}} = x_{\text{end}} - x_{\text{start}} = v_{\text{HV}}s_c/v_r, \tag{26}$$

where v_r is a reference velocity and s_c is a scaling constant.

At higher speeds, a large longitudinal-to-lateral ratio may lead to abrupt lateral motion and reduced comfort. To mitigate this effect, the longitudinal displacement is adjusted as

$$s^*_{\text{lon}} = s_{\text{lon}} - w\cdot\tan(\arctan(w/s_{\text{lon}})+c)^{-1},$$

where w is the lane width and c is a tuning constant. The optimized endpoint (x_e^*, y_e^*) is then computed using the adjusted longitudinal displacement.

Finally, intermediate waypoints are recursively inserted between the start and end points until the spacing between consecutive points satisfies a predefined threshold, yielding a smooth and dynamically feasible lane-change trajectory.

TABLE II: MPC TUNING PARAMETERS

Parameter	Value	Description
T_s, N_p, N_c	0.1 s, 10, 5	Sampling time, prediction horizon, control horizon
$\mathbb{X}$	1	Weight on longitudinal position error
$\mathbb{Y}$	10	Weight on lateral deviation (lane centering)
$\mathbb{V}$	2	Weight on velocity error (speed tracking)
$\mathbb{U}$	0.1	Weight on control-input changes (smooth actuation)

VII. Control Process

In our approach, MPC is used during lane changing to follow pre-defined trajectories, optimizing control in advance to reduce computation and ensure accuracy. The game-theoretic module determines the maneuver decision and timing at a high level, while MPC is employed solely for low-level trajectory tracking and control execution, ensuring dynamic feasibility and comfort. The discretized vehicle model for MPC is derived using the Euler method with sample time T_s and given as

$$\begin{aligned}
x(k+1) &= x(k) + v(k)\cos(\varphi(k))T_s,\\
y(k+1) &= y(k) + v(k)\sin(\varphi(k))T_s,\\
\varphi(k+1) &= \varphi(k) + v(k)\tan(\delta(k))T_s/L,\\
v(k+1) &= v(k) + \Delta v(k)T_s,\\
\delta(k+1) &= \delta(k) + \Delta\delta(k)T_s,
\end{aligned} \tag{27}$$

where $\Delta v(k)$ and $\Delta\delta(k)$ are the changes in velocity and steering angle between steps k and $k-1$ with input $\Delta u = [\Delta v(k), \Delta\delta(k)]^\top$. The MPC problem is formulated as

$$\begin{aligned}
&\min \quad J_{\text{mpc}} \qquad (28)\\
&\text{s.t. } (27), 0 < v(k+i) \le v_{\max}, a_{\min} \le \Delta v(k+i)/T_s \le a_{\max},\\
&\delta_{\min} \le \delta(k+i) \le \delta_{\max},\ \dot{\delta}_{\min} \le \Delta\delta(k+i)/T_s \le \dot{\delta}_{\max},
\end{aligned}$$

where $J_{\text{mpc}} = \sum_{i=1}^{N_p}\|\tilde{x}(k+i) - d_{\text{safe}}\|^2_{\mathbb{X}} + \|\tilde{y}(i)\|^2_{\mathbb{Y}} + \|\tilde{v}(i)\|^2_{\mathbb{V}} + \sum_{i=0}^{N_c-1}\|\Delta u(k+i)\|^2_{\mathbb{U}}$ is the cost function; $\tilde{x}$, $\tilde{y}$ and $\tilde{v}$ represent deviations in longitudinal position, lateral position, and velocity from their reference values. Definition of the MPC parameters are listed in Table II.

This article has been accepted for publication in IEEE Transactions on Consumer Electronics. This is the author's version which has not been fully edited and content may change prior to final publication. Citation information: DOI 10.1109/TCE.2026.3675966

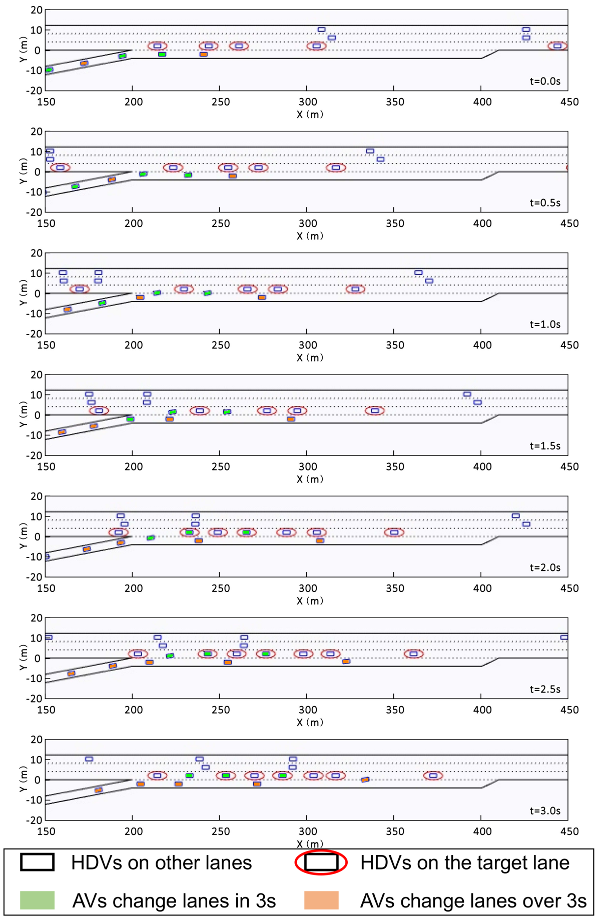

Fig. 5: Interactive driving with conservative HDVs.

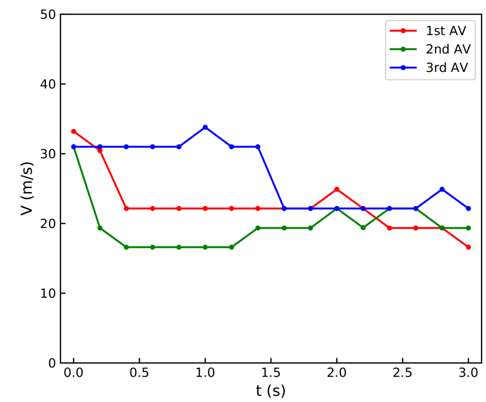

Fig. 6: AVs' velocities: conservative HDVs.

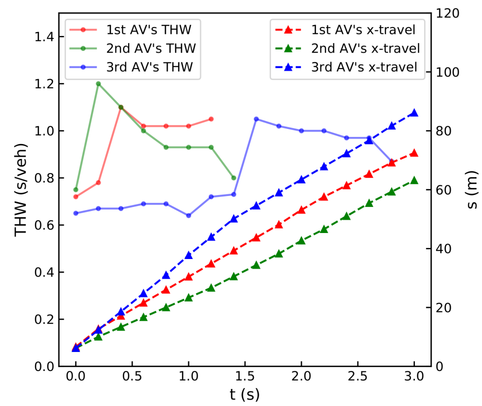

Fig. 7: Longitudinal distance and THW: conservative HDVs.

VIII. Simulation Results

This section evaluates the proposed framework in interactive ramp-merging scenarios with mixed traffic and heterogeneous driving styles. Experiments are conducted in MATLAB 2022b using a ramp simulation environment.

1) Experimental Setup: The road length is 300 m with lane width $4\ \mathrm{m}$. Standard vehicles are modeled as $4 \times 1.8\ \mathrm{m}$, and long vehicles as $10 \times 2\ \mathrm{m}$. Simulations run at $0.2\ \mathrm{s}$ resolution with traffic demand of 200 $\mathrm{vehicles/h}$ on the ramp and 100 $\mathrm{vehicles/h}$ on the main road. Vehicle speeds are bounded within $[0, 57]\ \mathrm{m/s}$. Three driving styles (conservative, moderate, aggressive) correspond to efficiency demand intervals of 0–25%, 25.1–52%, and 52.1–100%, respectively. Style recognition is based on ITTC and THW; given identical initial longitudinal speeds, ITTC serves as the dominant discriminator. Representative speeds derived from NGSIM are set to 7.1, 21.9, and 43.3 $\mathrm{m/s}$, while the AV initial speed is uniformly sampled from 20–40 $\mathrm{m/s}$. In Eq.(4), we use $w_1 = 0$, $w_2 = 0.5$, and $w_3 = 1$ to emphasize safety and efficiency. Each merge lasts approximately 3 s, during which driving styles are assumed fixed. Dynamic lane-changing intentions are captured by the unsatisfactory level in (1), enabling real-time adaptation to gap and speed conditions.

2) Interactive Driving with Conservative HDVs: Figure 5 illustrates AV performance when conservative HDVs occupy the target lane. Over the 3 s horizon, several AVs attempt to merge but are initially blocked by limited gaps. The 2nd AV merges at 0.5 s, followed by the 2nd and 3rd AVs by 1 s, while the 1st AV remains on the ramp and adjusts its position behind the rear target-lane vehicle. The 5th AV enters at 2 s and merges by 2.5 s. By 3 s, the 1st AV completes its lane change, resulting in three AVs successfully merged. Overall, conservative HDVs restrict lane-changing space, necessitating delayed maneuvers and highlighting the effectiveness of the proposed game-based method.

Figure. 6 illustrates the velocities of three AVs that enter the target lane in 3 s. The 1st AV reduces its speed from 33 $\mathrm{m/s}$ to 22 $\mathrm{m/s}$ within the first 0.5 s, maintains approximately 22 $\mathrm{m/s}$ from 0.5 to 2 s, and then decreases to around 16 $\mathrm{m/s}$ during the final second. The 2nd AV drops from 31 $\mathrm{m/s}$ to 16 s in the first 0.5 s, holds nearly constant between 0.5 s and 1.2 s, and fluctuates around 20 $\mathrm{m/s}$ thereafter. The 3rd AV maintains about 30 $\mathrm{m/s}$ for the first 1.5 s before settling at 22 $\mathrm{m/s}$ for the remainder of the interval. Fig. 7 illustrates the longitudinal displacements and THW before entering into the target lane of three AVs. According to [28], THW over 1 can be considered as no risk of collisions. Three AVs can reach the safety THW from the initial THW level around 0.4 s, 0.1 s and 1.6 s, which increases the driving safety. It can be observed that the 1st AV has a longer longitudinal distance, around 80 m, than the other two AVs. This is in accordance with more adjustments of the 1st AV during the driving. All AVs keep increasing their longitudinal distance stably, ensuring stable driving efficiency.

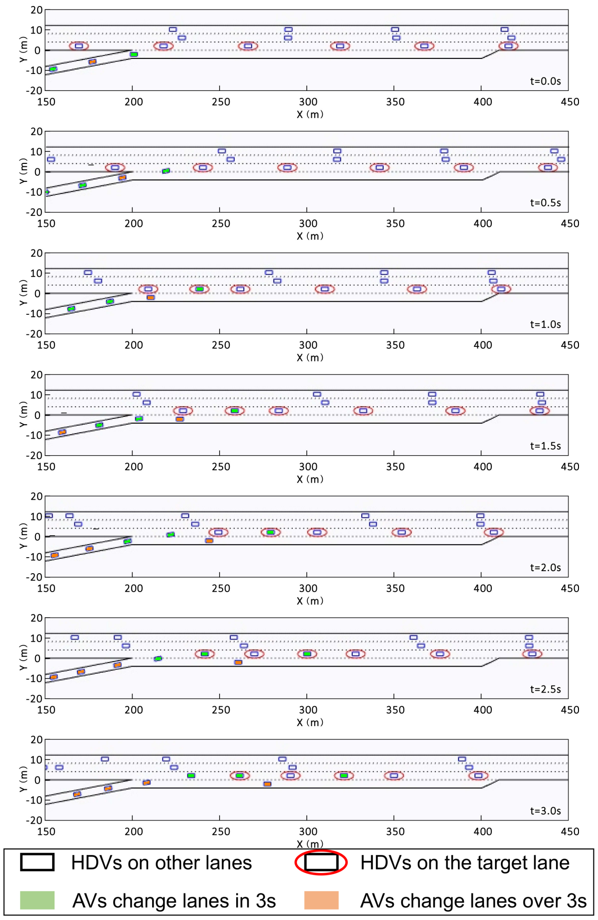

Fig. 8: Interactive driving with moderate HDVs.

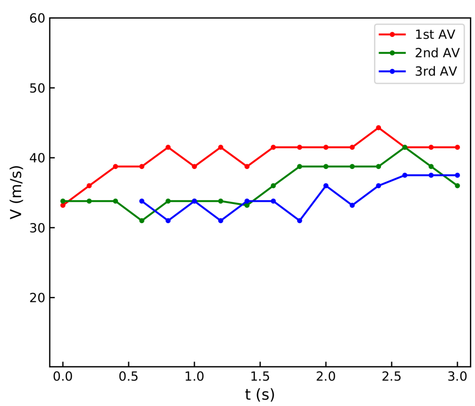

Fig. 9: AVs' velocities: moderate HDVs.

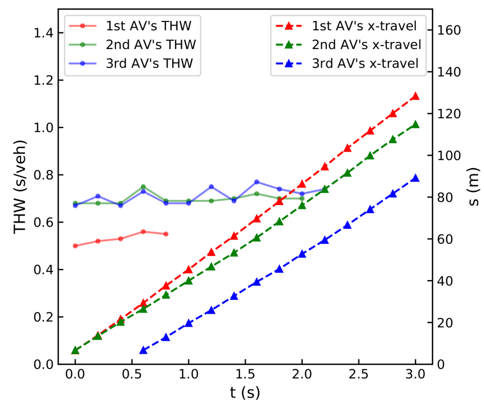

Fig. 10: Longitudinal distance and THW: moderate HDVs.

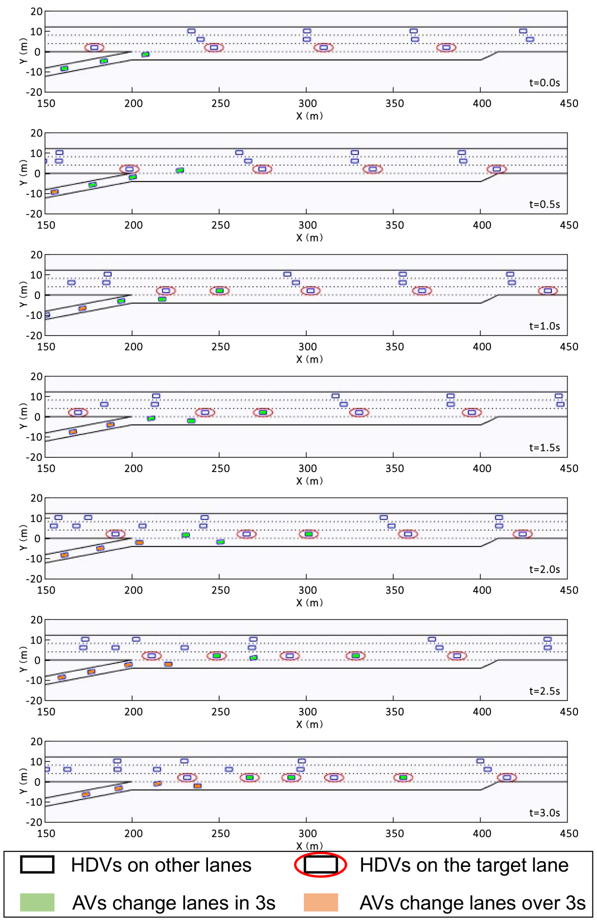

Fig. 11: Interactive driving with aggressive HDVs.

3) Interactive Driving with Moderate HDVs: Figure 8 shows AVs' performance when moderate HDVs are on the target lane, over a 3 s duration. At 0 s, the 1st AV enters the ramp lane, with HDVs ahead and behind on the target lane. At 0.5 s, the 1st AV merges into the target lane. By 1 s, the 2nd AV is still on the ramp. At 1.5 s, the 2nd AV waits for a safe merging opportunity, while the 3rd AV enters the ramp. At 2 s, the 2nd AV adjusts its position, and the 3rd AV merges into the target lane. By 2.5 s, the 3rd AV is fully in the target lane, and the fourth AV starts merging. At 3 s, the fourth AV enters the target lane. All AVs successfully choose proper times for lane changes, demonstrating the effectiveness of the proposed game-based framework for moderate HDVs.

Figure 9 shows the velocities of three AVs entering the target lane in 3 s. The 1st AV reaches 40 m/s in 0.6 s and maintains it throughout. The 2nd AV reaches about 35 m/s in 1.5 s and stays near 40 m/s after. The 3rd AV varies around 35 m/s for 2.2 s and increases to 37 m/s. The AVs in this scenario show higher average speeds than those with conservative HDVs, proving efficacy of the proposed method. Fig. 10 shows the longitudinal distance and THW before entering the target lane. The 1st AV changes lanes quickly,

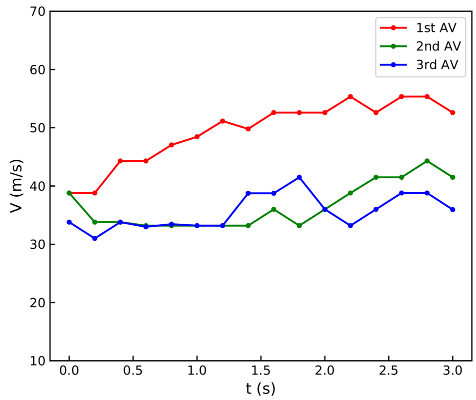

Fig. 12: AVs' velocities: aggressive HDVs.

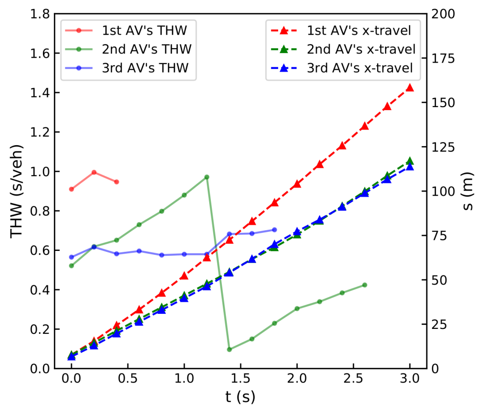

Fig. 13: Longitudinal distance and THW: aggressive HDVs.

with THW increasing from 0.5 to 0.57. The 2nd AV has a higher initial THW and decreases it from 0.7 to 0.58 as the front vehicle changes. The 3rd AV maintains a THW of around 0.75 before lane changing. All three AVs exhibit stable, gradual increases in longitudinal distance, reflecting the efficiency of the proposed framework for moderate HDVs.

4) Interactive Driving with Aggressive HDVs: Figure 11 shows the driving performance of AVs when aggressive HDVs are on the target lane over a 3 s duration. At 0 s, one AV enters the target lane. By 0.5 s, the 2nd AV merges into the ramp lane while the 1st AV enters the target lane. At 1 s, the 2nd AV is adjusting for lane changing due to limited longitudinal distance to the HDV. By 1.5 s, it's still waiting for a safe time point, and the 3rd AV merges into the ramp lane. By 2 s, the 2nd AV adjusts its position, and the 3rd AV enters the target lane. By 2.5 s, the 2nd AV enters the target lane. At 3 s, all three AVs are stably in the target lane, having selected proper lane-changing times. This demonstrates the intelligence of AVs using the proposed game-based framework.

Figure 12 shows the velocity variation of three AVs entering the target lane in 3 s. The 1st AV accelerates from 40 m/s to 55 m/s, while the 2nd AV decelerates from 40 m/s to 34 m/s in 1.8 s, then increases its speed to around 42 m/s. The 3rd AV increases its velocity from 30 to 34m/s in 1.25 s, then oscillates around 35 m/s for the remainder. Fig. 13 shows the longitudinal distance and THW before entering the target lane for three AVs. The 1st AV completes lane changing quickly, maintaining a THW above 1, indicating high safety.

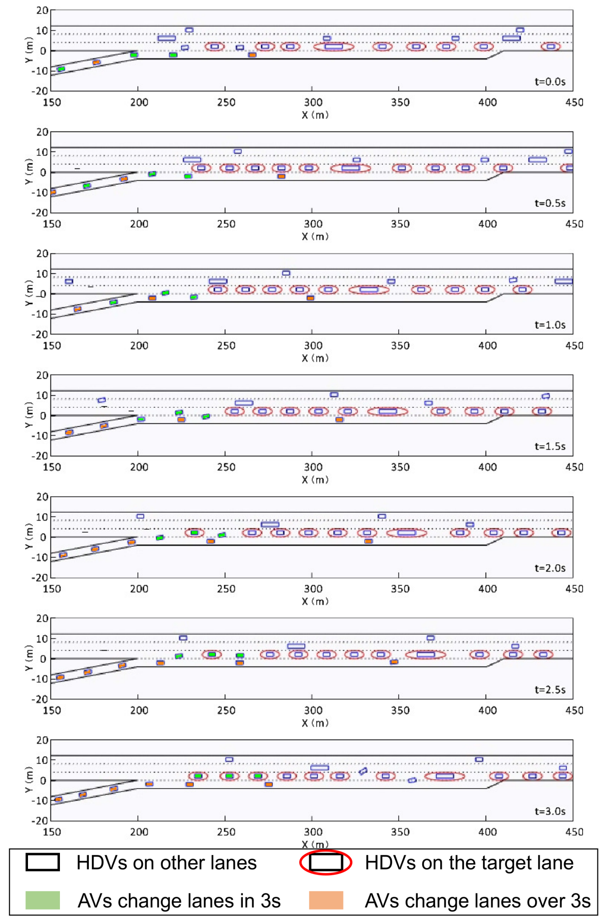

Fig. 14: Interactive driving with mixed traffic.

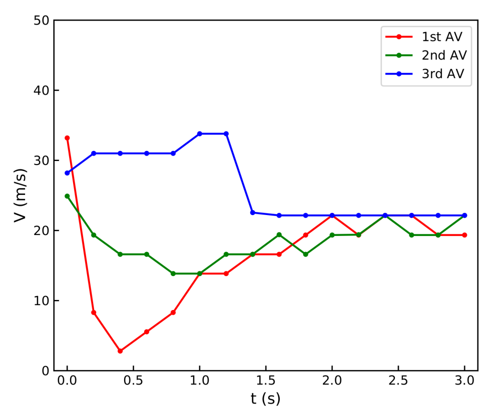

Fig. 15: AVs' velocities: mixed traffic.

The 2nd AV reaches a THW of 1 at 1 s, and at 1.2 s, the decision to change lanes shifts from the ramp lane to the target lane, causing abrupt changes in THW. Despite this, collision detection confirms the decision is safe. The 3rd AV maintains a THW around 0.7 before lane changing, ensuring relatively high safety. All three AVs exhibit stable, gradually increasing longitudinal distances. The second and 3rd AVs end with the same final distance, as the 2nd AV spends more time adjusting its position for lane changing.

5) Mixed Traffic Flow with Moderate HDVs: This section evaluates the proposed method in mixed traffic with moderate

This article has been accepted for publication in IEEE Transactions on Consumer Electronics. This is the author's version which has not been fully edited and content may change prior to final publication. Citation information: DOI 10.1109/TCE.2026.3675966

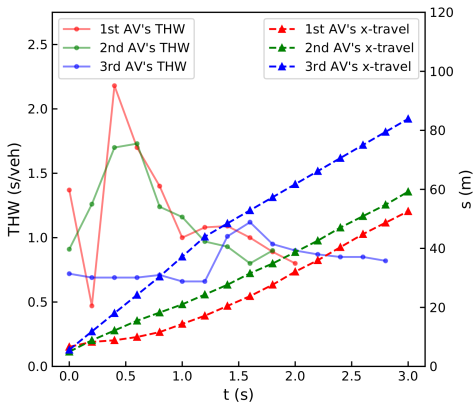

Fig. 16: Longitudinal distance and THW: mixed traffic.

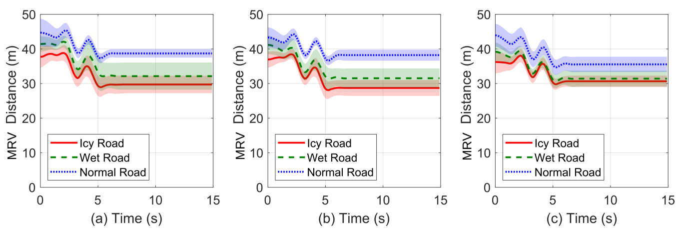

Fig. 17: Mean relative vehicle (MRV) distances ($N = 10$ runs) under nine slope–surface conditions.

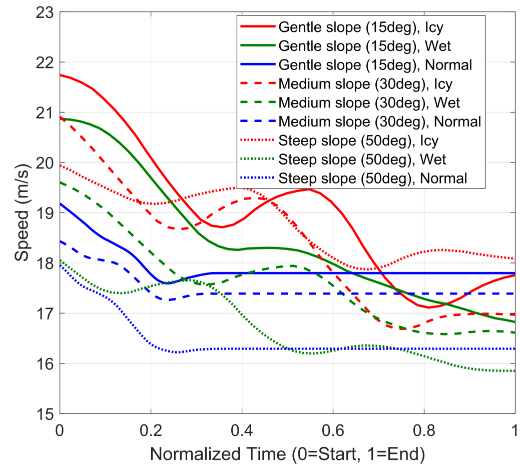

Fig. 18: Mean velocities during lane change under nine slope–surface combinations in dense traffic.

TABLE III: LANE CHANGING PERFORMANCE

Scenario	Time [s]		Speed [m/s]		THW [s/veh]		Collisions	
	Ours	[29]	Ours	[29]	Ours	[29]	Ours	[29]
Conservative HDVs	**1.42**	1.85	**17.39**	14.54	0.95	1.21	**0**	16
Moderate HDVs	**0.86**	1.62	**36.68**	17.30	0.53	1.15	0	0
Aggressive HDVs	**0.81**	0.86	**39.45**	38.06	0.46	0.83	0	0
Mixed platoon	**1.12**	1.26	22.15	22.39	**0.97**	0.87	**0**	14

HDVs over a 3 s horizon (Fig. 14). Initially, two AVs are on the ramp and a third enters. The 3rd AV merges by 0.5 s, while the 1st and 2nd AVs remain constrained by limited safe gaps. The 4th–6th AVs enter sequentially, and by 3 s, three AVs have stably merged into the target lane. Fig. 15 shows the velocity profiles. The 1st AV decelerates from 35 to 30 $\mathrm{m/s}$ within 0.4 s and stabilizes around 22.5 $\mathrm{m/s}$. The 2nd AV oscillates between 14 and 25 $\mathrm{m/s}$, whereas the 3rd AV accelerates from 28 to 31 $\mathrm{m/s}$ before converging to a similar steady speed. Fig. 16 reports longitudinal distances and THW before lane changes. The 1st and 2nd AVs maintain THW above 1, indicating high safety, while the 3rd AV remains above 0.7. Overall, the 3rd AV achieves the largest progress with fewer safety constraints, whereas the others merge more conservatively.

6) Validation on Various Merging Situations: To validate effectiveness of the proposed framework under different road conditions, we conducted simulations across three slopes (15°, 30°, and 50°) and three road surface conditions with friction coefficients of $\mu = 0.8$ (normal), $\mu = 0.5$ (wet), and $\mu = 0.15$ (icy). For each of the nine combinations, we performed $N = 10$ independent runs with randomized initial conditions. Each trial included one AV and one HDV in the target lane, with the AV's initial velocity sampled as $v_{\mathrm{AV}} \sim \mathcal{U}(17, 23)$ $\mathrm{m/s}$ and the HDV's velocity as $v_{\mathrm{HDV}} \sim \mathcal{U}(12.5, 17.5)$ $\mathrm{m/s}$. The HDV's starting position was randomized as $\Delta x \sim \mathcal{U}(-7.5, 7.5)$ m relative to its nominal midpoint.

Figure 17 shows the mean relative vehicle (MRV) distances over 10 runs under nine slope-surface conditions. On icy roads, the distance starts at approximately 38 m, fluctuates between 2–6 seconds with a minimum of about 30 m, and stabilizes around 28–29 m after 8 s. On wet roads, the distance begins at approximately 38–39 m, decreases with similar fluctuations to icy roads between 2–6 s, reaching about 32 m, and stabilizes around 31–32 m after 8 s. On normal roads, the distance starts highest at about 45 m, experiences noticeable fluctuations between 2–6 s with peaks at approximately 43–45 m and troughs at about 39–40 m, and stabilizes around 38–39 m after 8 s. Fig. 18 shows the AV's mean velocities, time-normalized from merge start to end, across nine slope and surface conditions in dense traffic. On gentle slopes, the AV on normal pavement accelerates to about 19.2 $\mathrm{m/s}$, then decelerates to 17.8 $\mathrm{m/s}$. On wet surfaces, it peaks at 21 $\mathrm{m/s}$, settling at 16.7 $\mathrm{m/s}$, and on icy roads, it starts at 22 $\mathrm{m/s}$, holding at 17.7 $\mathrm{m/s}$. For medium slopes, the normal profile peaks at 18.5 $\mathrm{m/s}$ and ends at 17.5 $\mathrm{m/s}$, the wet profile peaks at 19.5 $\mathrm{m/s}$ and ends at 16.4 $\mathrm{m/s}$, and icy roads peak at 21 $\mathrm{m/s}$ and end at 17 $\mathrm{m/s}$. On steep slopes, the normal and wet profiles start near 18 $\mathrm{m/s}$ but dip more sharply, with normal reaching 16.3 $\mathrm{m/s}$ and wet ending at 17.8 $\mathrm{m/s}$. The icy profile starts at 20 $\mathrm{m/s}$ and ends at 18 $\mathrm{m/s}$.

7) Comparison with Existing Methods: We compare our method with the simpler model in [29], which uses basic gap acceptance without considering driving styles or uncertainty. Table III summarizes lane-changing time, speed, THW, and collisions, with each scenario tested ten times using random HDV speeds. While the baseline performs reasonably in simple cases, it struggles in complex ones—causing 16 collisions in conservative HDV scenarios. In contrast, our method consistently achieves shorter lane-change times (up to 46.9% faster) and significantly higher speeds (up to 111.4%), demonstrating clear safety and performance gains. We further benchmark our method against recent studies [30], [31], [32], [33], as shown in Table IV. While existing methods address

TABLE IV: COMPARISON WITH EXISTING METHODS

Methods	Scenario	ML	ID	UP	CD	MTSV	VT
[30]	Ramp	√	-	√	-	-	√
[31]	Ramp	-	√	-	-	-	√
[32]	Ramp	√	-	-	-	-	√
[33]	Ramp	√	-	-	-	-	√
Ours	Ramp	√	√	√	√	√	√

MLR: Multi-lane ramp, ID: Interactive driving, UP: Uncertainty process, CD: Collision detection, MTSV: Multiple types of surrounding vehicles, VT: Verified in traffic flow, -: not considered or not given.

TABLE V: COMPUTATIONAL PERFORMANCE

Algorithm	Runtime (ms)			Memory (KB)			Energy (mJ)		
	Light	Mod.	Dense	Light	Mod.	Dense	Light	Mod.	Dense
Ours	**0.02**	**0.02**	**0.03**	**0.1**	**0.1**	**0.1**	**0.04**	**0.04**	**0.06**
MFG-MPC	0.48	0.57	0.74	32.5	39.1	48.6	0.96	1.14	1.48
MCDP	4.92	7.19	16.78	780.2	1570.3	3920.5	9.84	14.38	33.56
RFSG	0.41	0.50	0.72	21.3	26.0	34.7	0.82	1.00	1.44

aspects like multi-lane ramps or interactive driving, they often overlook uncertainty, collision detection, or vehicle diversity. In contrast, our approach integrates all these factors, making it better suited for complex, real-world ramp scenarios. The added complexity is justified by improved safety and efficiency where benchmarks fall short.

A. Consumer Electronics Platform Evaluation

To validate the suitability of the proposed method, we conduct computational benchmarks comparing runtime, memory footprint, and energy efficiency against three representative baselines: Mean Field Game with MPC (MFG-MPC) [34], Monte Carlo Decision Process (MCDP) [35], and Risk Field Stackelberg Game (RFSG) [36].

1) Experimental Setup: Simulations were conducted on a Ubuntu OS equipped with an Intel Core i5-12600KF CPU, an NVIDIA RTX 3070Ti GPU, and 16 GB RAM. All experiments were implemented in MATLAB R2024b to evaluate computational feasibility under consumer-grade onboard resources. Three traffic scenarios with 5, 10, and 15 surrounding HDVs were tested, each repeated over 100 trials.

2) Runtime Analysis: Table V reports the average runtime across different traffic densities. Under light, moderate, and high traffic conditions (5, 10, and 15 HDVs), the proposed GEE method achieves an average runtime of **0.02 ms**, operating consistently at a sub-millisecond scale. In comparison, MFG-MPC, RFSG, and MCDP require 0.57 ms, 0.50 ms, and 7.19 ms, respectively. This corresponds to runtime reductions of approximately **96.5%** relative to MFG-MPC, **96.0%** relative to RFSG, and over **99.7%** relative to MCDP.

3) Memory Footprint: Memory usage is reported as the estimated peak size of major allocated arrays, providing a platform-independent comparison. Under moderate traffic, GEE requires only **0.1 KB**, reflecting its lightweight $\mathcal{O}(N)$ structure. In contrast, MFG-MPC and RFSG consume 39.1 KB and 26.0 KB, respectively, due to grid-based state representations, while MCDP requires 1570.3 KB to store Monte Carlo trajectory samples. This corresponds to memory reductions of approximately **99.7%**, **99.6%**, and **99.99%** compared to MFG-MPC, RFSG, and MCDP, respectively, enabling deployment on resource-constrained ECUs.

4) Energy Consumption: Energy efficiency is evaluated using a normalized energy index computed as CPU runtime multiplied by a nominal processor power of 2 W, serving as a relative proxy rather than a direct power measurement. Under moderate traffic, GEE consumes **0.04 mJ** per decision cycle, compared to 1.14 mJ for MFG-MPC, 1.00 mJ for RFSG, and 14.38 mJ for MCDP. This represents energy reductions of approximately **96.5%**, **96.0%**, and **99.7%**, respectively. Over extended driving durations with frequent decision updates, such reductions contribute to lower thermal load and improved energy efficiency on consumer electronic platforms.

B. Discussion and Limitations

While the proposed framework demonstrates strong performance in interactive ramp-driving scenarios, several limitations should be acknowledged. First, the game-theoretic formulation assumes bounded rationality and predefined payoff structures for surrounding human-driven vehicles. Although these assumptions are widely adopted in interaction-aware planning, real human behavior may deviate from rational or stationary decision-making, especially under extreme or unexpected conditions.

Second, the proposed model focuses on local interactions within a limited spatial and temporal horizon, which is suitable for time-critical ramp merging but may not fully capture long-term strategic behaviors in more complex traffic networks. Extending the framework to multi-stage or hierarchical games could further improve its applicability in large-scale scenarios.

Third, the performance of the GT-based decision module depends on the design of payoff weights and uncertainty parameters. While our chosen parameters are grounded in empirical observations and validated through extensive simulations, adaptive or learning-based tuning mechanisms could further enhance robustness across diverse traffic conditions.

Finally, the current framework is evaluated primarily in simulation environments. Although the computational evaluation demonstrates strong suitability for consumer-grade electronic platforms, future work will focus on real-world deployment and hardware-in-the-loop testing to further validate robustness under sensing noise, communication delays, and model mismatch.

IX. Conclusion

This paper presented a top-down, interaction-aware planning framework for autonomous ramp driving that explicitly accounts for heterogeneous human driving styles and perception uncertainty. The proposed approach integrates data-driven driving style grading, uncertainty modeling via prediction error ellipses, game-theoretic time-point selection, and lightweight planning and control modules suitable for consumer-grade electronic platforms. Extensive simulation results under mixed traffic conditions demonstrate collision-free operation, stable velocity profiles, and improved merge efficiency, particularly in congested ramp scenarios. While the game-theoretic formulation provides a structured mechanism for interaction-aware decision-making, it is inherently limited by assumptions on human rationality and predefined payoff structures. Future work will focus on enhancing adaptability through learning-assisted or adaptive MPC-based trajectory generation, as well as validating the proposed framework in hardware-in-the-loop and real-world ramp-driving experiments for consumer electronic intelligent vehicles.

References

[1] Y. Yan, D. Han, Q. Zhang, J. Wang *et al.*, "Event-triggered personalized driving based on passenger's subjective risk evaluation," *IEEE Trans. Intell. Transp. Syst.*, vol. 26, no. 2, pp. 1982–1998, 2025.

[2] B. Peng *et al.*, "Communication scheduling by deep reinforcement learning for remote traffic state estimation with bayesian inference," *IEEE Trans. Veh. Technol.*, vol. 71, no. 4, pp. 4287–4300, 2022.

[3] Y. Liu, X. Pei, H. Zhou, and X. Guo, "Spatiotemporal trajectory planning for autonomous vehicle based on reachable set and iterative LQR," *IEEE Trans. Veh. Technol.*, vol. 73, no. 8, pp. 10 932–10 947, 2024.

[4] C. M. Martinez *et al.*, "Driving style recognition for intelligent vehicle control and advanced driver assistance: A survey," *IEEE Trans. Intell. Transp. Syst.*, vol. 19, no. 3, pp. 666–676, 2017.

[5] Z. Tian *et al.*, "Efficient and balanced exploration-driven decision making for autonomous racing using local information," *IEEE Trans. on Intell. Veh.*, pp. 1–17, 2024.

[6] X. Hu *et al.*, "Autonomous vehicle's impact on traffic: Empirical evidence from waymo open dataset and implications from modelling," *IEEE Trans. Intell. Transp. Syst.*, vol. 24, no. 6, pp. 6711–6724, 2023.

[7] P. Hang *et al.*, "Decision making of connected automated vehicles at an unsignalized roundabout considering personalized driving behaviours," *IEEE Trans. Veh. Technol.*, vol. 70, no. 5, pp. 4051–4064, 2021.

[8] X. Wang, J. Han, Y. Liu, H. Shi, L. Chen, F. Zhong, and S. Liu, "A dynamics model for driving behavior based on coupling actuation of bounded rational cognition and diverse emotions," *Transp. Res. Part C: Emerg. Technol.*, vol. 159, p. 104479, 2024.

[9] N. Djuric, V. Radosavljevic, H. Cui, T. Nguyen *et al.*, "Uncertainty-aware short-term motion prediction of traffic actors for autonomous driving," in *Proc. WACV*, 2020, pp. 2084–2093.

[10] Z. Lin, J. Lan, A.-T. Nguyen, and D. Flynn, "Contingency-aware spatiotemporal optimization for safe autonomous vehicle trajectory planning," *IEEE Trans. Intell. Transp. Syst.*, pp. 1–13, 2025.

[11] Y. Wang, N. Lyu, and J. Wen, "Game theory-based mandatory lane change model in intelligent connected vehicles environment," *Applied Mathematical Modelling*, vol. 132, pp. 146–165, 2024. [Online]. Available: https://www.sciencedirect.com/science/article/pii/S0307904X24002063

[12] H. Vijayakumar, D. Zhao, J. Lan, W. Zhao *et al.*, "A holistic safe planner for automated driving considering interaction with human drivers," *IEEE Trans. Intell. Veh.*, vol. 9, no. 1, pp. 2061–2076, 2023.

[13] X. Chen, G. Qin, T. Seo, J. Yin, Y. Tian, and J. Sun, "A macro-micro approach to reconstructing vehicle trajectories on multi-lane freeways with lane changing," *Transp. Res. Part C: Emerg. Technol.*, vol. 160, p. 104534, 2024.

[14] N. Iwahashi, "Equilibrium selective role coordination for autonomous driving," in *Proc. iCAST*, 2019, pp. 1–8.

[15] G. Liu, B. Xiao, and D. Li, "Game-theory based driving decision algorithm for intersection scenarios considering driver irrationality," in *Proc. CVCI*, 2020, pp. 747–752.

[16] C. Zhong *et al.*, "Self-adapting trajectory planning method considering joint constraints," in *Proc. ICCRE*. IEEE, 2022, pp. 277–283.

[17] Y. Jiang, H. Chen, G. Xiao, H. Cong, and Z. Yao, "A stackelberg game-based on-ramp merging controller for connected automated vehicles in mixed traffic flow," *Transportation Letters*, vol. 17, no. 3, pp. 423–441, 2025.

[18] Y. Jiang, Z. Man, Y. Wang, and Z. Yao, "Cooperative lane-changing for connected autonomous vehicles merging into dedicated lanes in mixed traffic flow," *Expert Systems with Applications*, vol. 252, p. 124163, 2024.

[19] Y. Jiang, Z. Man, K. Xia, Y. Wu, Y. Wang, and Z. Yao, "Model predictive control–based cooperative lane-changing strategy for connected autonomous vehicle platoons merging into dedicated lanes," *Expert Systems with Applications*, vol. 278, p. 127274, 2025.

[20] L.-y. Zhang *et al.*, "Simulation study on ramp inflow for hybrid autonomous driving," *Physical Communication*, vol. 55, p. 101932, 2022.

[21] J. Wu, Y. Wang, Z. Zhang, Y. Wen, L. Zhong, and P. Zheng, "A cooperative merging control method for freeway ramps in connected and autonomous driving," *Sustainability*, vol. 14, no. 18, p. 11120, 2022.

[22] J. Rios-Torres *et al.*, "Impact of partial penetrations of connected and automated vehicles on fuel consumption and traffic flow," *IEEE Transactions on Intelligent Vehicles*, vol. 3, no. 4, pp. 453–462, 2018.

[23] M. Khayyat, S. Bolognani, S. Arrigoni, and F. Braghin, "A sampling-based approach to urban motion planning games with stochastic dynamics," *IEEE Trans. Intell. Veh.*, pp. 1–15, 2024.

[24] M. Yuan, J. Shan, and H. Schofield, "Scalable game-theoretic decision-making for self-driving cars at unsignalized intersections," *IEEE Trans. Ind. Electron.*, vol. 71, no. 6, pp. 5920–5930, 2024.

[25] J. Hui and L. Ming, "Driving style recognition based on the score coefficient under the following condition," *J. Beijing Inst. Technol.*, vol. 41, no. 3, pp. 245–250, 2021.

[26] N. Lyu *et al.*, "Using naturalistic driving data to identify driving style based on longitudinal driving operation conditions," *J. Intell. Connect. Veh.*, vol. 5, no. 1, pp. 17–35, 2022.

[27] C. Lv *et al.*, "Driving-style-based codesign optimization of an automated electric vehicle: A cyber-physical system approach," *IEEE Trans. Ind. Electron.*, vol. 66, no. 4, pp. 2965–2975, 2018.

[28] D. Swaroop *et al.*, "A review of constant time headway policy for automatic vehicle following," in *Proc. ITSC*, 2001, pp. 65–69.

[29] Q. I. Yang *et al.*, "A microscopic traffic simulator for evaluation of dynamic traffic management systems," *Transportation Research Part C: Emerging Technologies*, vol. 4, no. 3, pp. 113–129, 1996.

[30] J. Zhu *et al.*, "Bi-level ramp merging coordination for dense mixed traffic conditions," *Fundamental Research*, 2023.

[31] Z. e. a. Kherroubi *et al.*, "Novel decision-making strategy for connected and autonomous vehicles in highway on-ramp merging," *IEEE Trans. Intell. Transp. Syst.*, vol. 23, no. 8, pp. 12 490–12 502, 2022.

[32] H. Wang *et al.*, "Interpretable decision-making for autonomous vehicles at highway on-ramps with latent space reinforcement learning," *IEEE Trans. Veh. Technol.*, vol. 70, no. 9, pp. 8707–8719, 2021.

[33] J. Liu, W. Zhao, and C. Xu, "An efficient on-ramp merging strategy for connected and automated vehicles in multi-lane traffic," *IEEE Trans. Intell. Transp. Syst.*, vol. 23, no. 6, pp. 5056–5067, 2022.

[34] L. Zheng, X. Wang, F. Li, Z. Mao, Z. Tian, Y. Peng, F. Yuan, and C. Yuan, "A mean-field-game-integrated mpc-qp framework for collision-free multi-vehicle control," *Drones*, vol. 9, no. 5, p. 375, 2025.

[35] Z. Lin, J. Lan, C. Anagnostopoulos, Z. Tian, and D. Flynn, "Safety-critical multi-agent mcts for mixed traffic coordination at unsignalized intersections," *IEEE Transactions on Intelligent Transportation Systems*, vol. 26, no. 11, pp. 18 992–19 006, 2025.

[36] Z. Lin, Z. Tian, J. Lan, D. Zhao, and C. Wei, "Uncertainty-aware roundabout navigation: A switched decision framework integrating stackelberg games and dynamic potential fields," *IEEE Transactions on Vehicular Technology*, pp. 1–13, 2025.